Biosensors and Bioelectronics 24 (2008) 1–13

Contents lists available at ScienceDirect

Biosensors and Bioelectronics

journal homepage: www.elsevier.com/locate/bios

Review

Magnetic labeling, detection, and system integration

C.R. Tamanaha*, S.P. Mulvaney, J.C. Rife, L.J. Whitman

Naval Research Laboratory, Code 6177, 4555 Overlook Avenue, SW, Washington, DC 20375-5342, USA

ARTICLE INFO

Article history:
Received 21 December 2007
Accepted 8 February 2008
Available online 16 February 2008

Keywords:
Biosensor
Magnetic bead
Magnetic detection
Biomolecular labeling

ABSTRACT

Among the plethora of affinity biosensor systems based on biomolecular recognition and labeling assays, magnetic labeling and detection is emerging as a promising new approach. Magnetic labels can be non-invasively detected by a wide range of methods, are physically and chemically stable, relatively inexpensive to produce, and can be easily made biocompatible. Here we provide an overview of the various approaches developed for magnetic labeling and detection as applied to biosensing. We illustrate the challenges to integrating one such approach into a complete sensing system with a more detailed discussion of the compact Bead Array Sensor System developed at the U.S. Naval Research Laboratory, the first system to use magnetic labels and microchip-based detection.

Contents

* Corresponding author. Tel.: +1 202 404 2121; fax: +1 202 767 3321.
E-mail address: cy.tamanaha@nrl.navy.mil (C.R. Tamanaha).

0956-5663/$ – see front matter © 2008 Elsevier B.V. All rights reserved.
doi:10.1016/j.bios.2008.02.009

1. Introduction

Affinity biosensor systems based on biomolecular recognition and labeling assays are under intense development for many applications, including biodefense (Hindson et al., 2005), medical diagnostics (Gao et al., 2004), food safety, and environmental monitoring (Baeumner, 2003; Farre and Barcelo, 2003). A general goal of labeled bioassays is to combine the innate sensitivity and specificity present in nature with an easily detectable taggant. As such, the most common approach to biosensing is the implementation of solid-phase binding assays whereby a chemical label that produces an externally observable signal is attached to a biomolecular target captured on a solid substrate. Traditionally, this attachment is accomplished using biomolecular recognition between the target molecule and a specific receptor (e.g. an antibody) that incorporates a label, or "reporter," such as a fluorophore, radioisotope, enzyme, nanoparticle, or electrochemically active species. To detect these reporter labels, a number of transduction mechanisms have been devised including optical, electrical, electrochemical, thermal, and piezoelectrical, all of which are covered eloquently by numerous reviews (see, for example, Pearson et al., 2000; Vo-Dinh and Cullum, 2000).

Out of the wide choice of labels that can be applied to common assay schemes, magnetic particles offer some unique advantages. The understanding of single magnetic particles goes back to 1949 and the pioneering work of Néel (1949). A few decades later, the concept of using magnetic particles as biomolecular labels was proposed (Dreyer, 1974). Presently, over 50 years after Néel, there is a growing interest in magnetic labels because of their potential detection by relatively non-invasive methods, their physical and chemical stability, their inexpensive methods of production, their environmental safety, and their biocompatibility. Here we provide an overview (*not* a comprehensive literature review) of the various approaches developed for magnetic labeling and detection as applied to biosensing. We illustrate the challenges to integrating one such approach into a complete sensing system with a more detailed discussion of the compact Bead Array Sensor System (*cBASS*®) incorporating the Bead ARray Counter (BARC®) sensor chip developed in our laboratory at the U.S. Naval Research Laboratory (NRL).

2. Biomolecular labeling with magnetic particles

Magnetic particle labels and magnetoelectronic detection offer a number of advantages for biosensing. Notably, there is no significant magnetic background present in most samples of interest, thereby enabling detection and magnetic manipulation, both *in vitro* and *in vivo*, without affecting the biological interactions. Microscale magnetic beads have been extensively developed over the past 15 years, primarily for cell and protein separation, and are available from a number of commercial sources. (Note that magnetic microbeads and their applications are the subject of the biennial *International Conference on Scientific and Clinical Applications of Magnetic Carriers* (http://www.magneticmicrosphere.com/meetings/)). A prime requirement for use as labels is that the beads must be paramagnetic or non-remanent to avoid clustering caused by residual magnetic moment in the absence of magnetic fields. One typical fabrication approach, used for Invitrogen's Dynal M-270, M-280, and M-450 micron-scale beads, is infusion of iron compounds into swollen polymer microparticles (Prestvik et al., 1997). Heat treatment results in 15–20 wt% Fe of iron-oxide ferromagnetic nanoparticles 20–40 nm in diameter distributed throughout the polymer matrix. The magnetic nanoparticles are single domain and small enough to be "superparamagnetic;" i.e., the thermal fluctuations at room temperature overcome lattice magnetic anisotropy forces, spontaneously randomizing the magnetization directions. Such magnetic microbeads can be prepared highly monodispersed in size. It has been observed that the magnetic content for Dynal M-280 beads 2.8 μm in diameter, while consistent on the average, varies from bead to bead with some beads even nonmagnetic (Rife et al., 2003). However, with the recent interest in magnetic bead labeled bioassays, manufacturers have started to offer beads with more consistent magnetic properties.

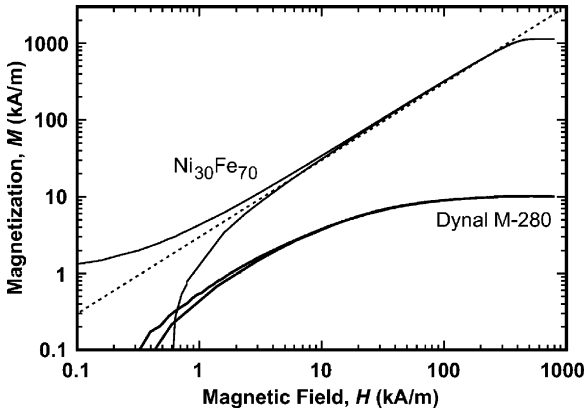

Fig. 1. Volume magnetization as a function of magnetic field for Dynal M-280 and $Ni_{30}Fe_{70}$ microbeads (solid lines) in a vibrating sample magnetometer. The dashed line shows the magnetization of an ideal paramagnetic sphere, $M = 3H$ (the theoretical maximum).

The average magnetization (magnetic moment/unit volume) versus applied magnetic field of Dynal M-280 beads (ca. 2002) is shown in Fig. 1. For improved magnetic signal strength, solid NiFe microbeads with 100% magnetic content have been investigated (Calvin et al., 2003). Perfect ferromagnetic spheres with diameters greater than about 0.2 μm in diameter can be multi-domain and non-remanent. The magnetization of the NiFe microbeads is also shown in Fig. 1, and shows considerable improvement in magnetization, with the magnetization approaching the maximum susceptibility possible for a paramagnetic sphere. The residual hysteresis and remanence below 1 kA/m (12.6 Oe) likely indicate small non-spherical deviations. Size sorting and surface functionalization require further development before these beads can be routinely applied in labeled bioassays.

3. Methods for detecting magnetic labels

A wide variety of methods have been developed for sensing and enumerating individual micron-scale magnetic particles. Magnetic materials have been used for decades in areas such as industrial sensor applications and data storage devices because of their versatility, ruggedness, and reliability. These applications have been the foundation of most of the magnetic field detection methods (both direct and indirect) developed for biosensing. The following are brief summaries covering representative magnetic detection strategies, roughly in chronological order, and segregated by the physical parameter measured.

3.1. Direct detection of magnetic particle labels

3.1.1. Magnetic permeability

3.1.1.1. Maxwell bridge. One of the earliest demonstrations of a binding assay detecting ferromagnetic labels is based on the measurement of magnetic permeability (Kriz et al., 1996). In this system shown in Fig. 2, a measuring coil (L_4) in a balanced Maxwell–Wien

bridge configuration is used to sense the presence of the ferromagnetic labels by referencing a calibrated resistor–capacitor pair (R_1C_1) in the bridge circuit.

The Maxwell bridge is energized by a sinusoidal wave and the output signal is measured as a voltage difference across the bridge at points *A* and *B*. The small voltage signal can be boosted with the addition of a differential operational amplifier circuit. Initially the bridge is balanced such that

$$L_4 = R_2R_3C_1 \quad (1)$$

and

$$R_4 = \frac{R_2R_3}{R_1}. \quad (2)$$

The inductance of a coil can be described by the following equation,

$$L = \left(\frac{\mu_r\mu_0A}{l}\right)N^2, \quad (3)$$

where μ_r represents the relative magnetic permeability of the material inside the coil, μ_0 is the permeability of vacuum, *A* is the cross sectional area of the coil, *l* is the length of the coil, and *N* is the number of coil turns. When magnetic material (in this case, dextran ferrofluid) is placed inside the coil, the magnetic permeability of the material changes the inductance of the coil, unbalances the Maxwell bridge, and causes a voltage difference to appear. The output signal from the bridge is proportional to the concentration of the magnetic material in the sample. Kriz et al. (1996) reported a measurement sensitivity of $21 \pm 4\,\mu V/(\mu g\,Fe/mL)$ and was able to demonstrate idealized direct, sandwich, and competitive binding immunoassays.

3.1.1.2. Frequency-dependent magnetometer. This device measures changes in the resonant frequency of a coil of wire when paramagnetic particles are placed inside the coil (Richardson et al., 2001). Like the device by Kriz et al. (1996), the effect that the magnetic particles have on the self-inductance, *L*, of a measuring coil is exploited (see Eq. (3)). However, in this method, a resonant inductor–capacitor (LC) circuit is used and the resonant frequency of the coil is measured with a circuit based on a voltage-controlled oscillator and a phase-locked loop (Fig. 3). The immunoassay used for this measurement method consists of standard plastic strips with paramagnetic particles on them. When the plastic strip is placed inside the measuring coil (which is connected in parallel with a capacitor), the presence of the particles causes the resonant frequency of the coil to decrease proportionally with the number of magnetic particles on the strip. The instrument is capable of detecting as few as 1×10^5 paramagnetic particles immobilized on a plastic strip and has a linear response ($r = 0.99$) for up to at least 3.33×10^6 particles. Recently, Kiely et al. (2007) reported an improved disposable biosensor constructed using PCB material and thick film processing techniques to create flat spiral measurement coils. They were able to demonstrate a Troponin I immunoassay with 0.5 ng/mL sensitivity.

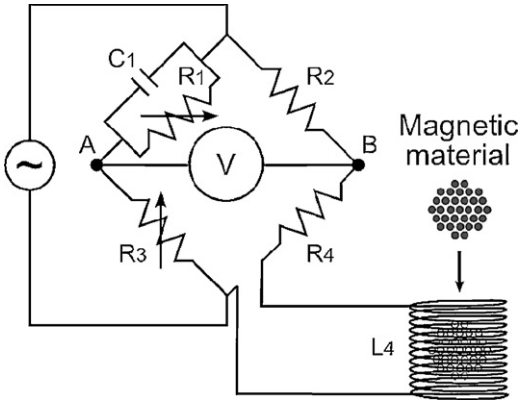

Fig. 2. Simplified schematic of a balanced Maxwell–Wien bridge configuration that senses the presence of magnetic material placed inside the coil (L_4).

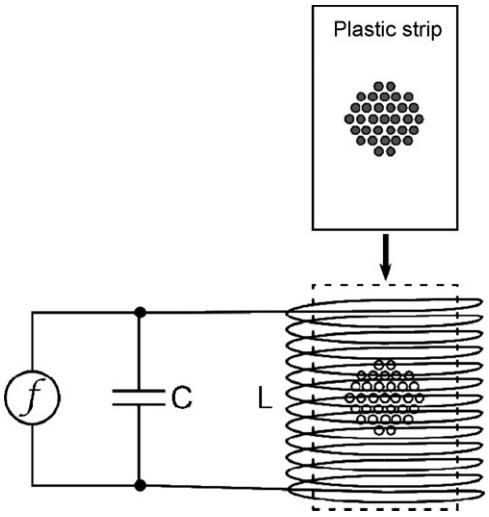

Fig. 3. The frequency-dependent magnetometer measures changes in the resonant frequency of a coil of wire when a plastic assay strip with immobilized paramagnetic beads is inserted inside the coil (L).

3.1.2. Magnetic remanence

3.1.2.1. Superconducting quantum interference device (SQUID). A SQUID sensor offers the highest sensitivity and largest dynamic range of all magnetic field measuring technologies. Kotitz et al. (1997) first introduced the concept of using a SQUID to detect antibodies labeled with magnetic nanoparticles as a way to avoid using radioisotopes or unstable enzymes or fluorescent dyes that are standard in immunoassays. As shown in Fig. 4, an externally applied magnetic field magnetizes the superparamagnetic nanoparticles

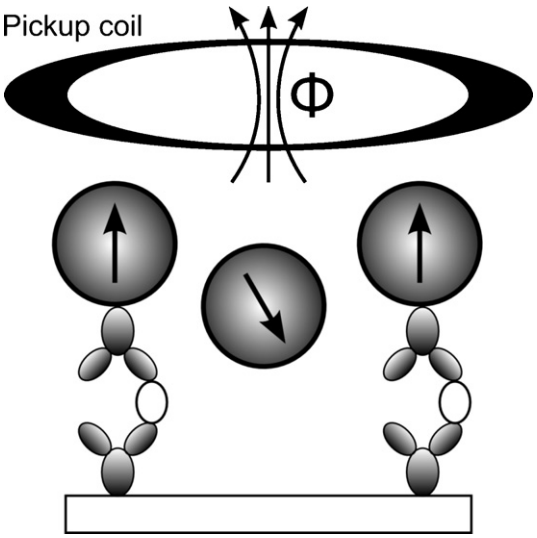

Fig. 4. A SQUID uses a superconducting pickup coil that measures the decay of the remanent magnetization of superparamagnetic nanoparticles bound to targets. Nanoparticles that are unbound relax very rapidly by Brownian rotation and do not contribute to the overall signal.

such that they line up along the magnetic field lines. When the magnetic field is removed, the particles remain aligned for a brief period before randomizing again. This short, but decaying, period of self-magnetization is described as magnetic remanence. A SQUID measures the decay of remanent magnetization of superparamagnetic nanoparticles bound to targets (~1 s), represented as the Néel relaxation time,

$$\tau_N = \tau_0 \exp\left(\frac{\Delta E}{kT}\right), \quad (4)$$

where τ_0 is the damping or excitation time (around 10^{-9} s), ΔE is the energy barrier (equal to KV, where K is the anisotropy constant of the bulk material and V is its volume), k is the Boltzmann's constant and T is the temperature. Nanoparticles that are unbound relax very rapidly (~1 ms) by Brownian rotation and therefore do not contribute to the overall signal,

$$\tau_B = \frac{3V_H\eta}{kT}, \quad (5)$$

where V_H is the hydrodynamic particle volume and η is the viscosity of the medium. Although the signal from a single particle can be detected, such sensitivity requires the particles to be in very close proximity or in contact with the sensor, and both the SQUID and the particle must be cooled to at least 77 K (−196 °C)—a major engineering challenge of this technology for biosensing applications.

A significant advance for this approach was the development of a high-transition temperature "SQUID microscope" that manages to maintain the SQUID detector at the required 77 K while allowing a sample at room-temperature and pressure to come as close as 40 μm to the SQUID detector (Black et al., 1995; Lee et al., 1996). By various improvements to the basic technique, Chemla et al. (2000), have reported a limit of detection of about 30,000 magnetic nanoparticles with an average core size of 35 ± 5 nm. Recently, in another SQUID measurement technique, Enpuku et al. (2005) and Tsukamoto et al. (2005) developed a 25 nm-diameter (nominal) Fe_3O_4 magnetic marker with a high magnetic field and designed an optimized pickup coil to detect the magnetic flux (Φ_s) signal from a moving sample. They reported the detection of 2 amol of IgE with this approach.

3.1.3. Magnetoresistance

In 1857, William Thomson (Lord Kelvin) first reported the anisotropic magnetoresistance (AMR) effect, observing that when iron was subjected to a magnetic field there was a 0.033% increase in its electrical resistance (Thomson, 1857). This very subtle effect is the result of the variation of an electron's mean free path as a function of the angle of the electron's velocity with respect to a conductive material's magnetization. The sensitivity of magnetoresistive (MR) materials is expressed as the change in resistance divided by the minimum resistance, or

$$\text{MRratio} = \frac{\Delta R}{R} = \frac{R - R_{Hsat}}{R_{Hsat}} \times 100\%, \quad (6)$$

where R_{Hsat} is the minimum resistance in a saturation field. Ratio comparisons are commonly reported for measurements taken at room temperature. It would be over a century, following the advent of thin-film technology, before this phenomenon could be applied in practical sensors; for example, in a readout transducer for magnetically recorded tapes (Hunt, 1971).

3.1.3.1. Giant magnetoresistance: coupled multiplayer. The giant magnetoresistive (GMR) effect was first described independently by Baibich et al. (1988) and Binasch et al. (1989) through the study of magnetic properties of magnetic and nonmagnetic metal thin-film multilayers. In a simplified view of a GMR device (Fig. 5),

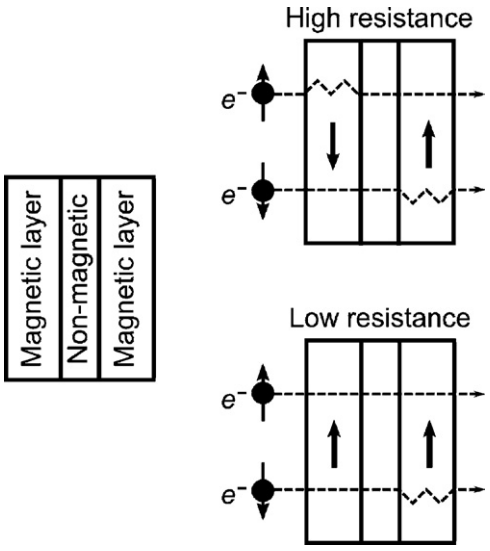

Fig. 5. The basic GMR concept. Overall resistance is relatively high when the orientation of the magnetic layers is in anti-parallel alignment, and relatively low when they are in parallel alignment. The orientation is important as it determines the "spin-dependent" scattering of electrons. For example, when the layers are aligned in parallel, scattering of all the "up" electrons is significantly reduced as they pass through the layers, yielding a lower overall resistance.

the resistance of two thin antiferromagnetically exchange-coupled layers separated by a thin nonmagnetic conducting layer can be altered by changing the moments of the ferromagnetic layers from anti-parallel to parallel. This change decreases the spin-dependent interfacial scattering of charge carriers resulting in a decrease in the resistance of the GMR material.

Simple multilayer GMR devices exhibit a magnetoresistance ratio between 4 and 9% (Caruso et al., 1998). Several important devices have utilized the phenomenon, most notably magnetic recording (read heads in hard drives) and magnetic non-volatile memory. Baselt et al. (1998) described a new concept in biological labeling and magnetic sensor detection based on GMR sensors. They described a semiconductor-based multilayer GMR sensor chip, which came to be known as the Bead ARray Counter, or BARC®, chip that detects local in-plane magnetic fields produced by paramagnetic microbeads immobilized directly above the sensor surface during binding assays. Over the past decade the sensor chip has been further developed into the BARC®-III chip with 64 sensing zones (Rife et al., 2003). Other investigators have also followed Baselt's initial approach with other GMR sensor devices (Schotter et al., 2002, 2004). The principles and operation of the NRL BARC® and its integration into a complete sensing system will be reviewed in detail below.

3.1.3.2. Giant magnetoresistance: spin-valve. Spin-valves also use the GMR magnetoresistive effect of spin-dependent interfacial scattering but with a somewhat different MR material stack. Spin-valves were first described by Dieny et al. (1991), but have more recently been used for magnetically-labeled biosensors by Graham et al. (2002, 2005) and Li et al. (2003, 2006). Graham et al. described a 2 μm × 6 μm sensor consisting of a MR material stack (Si/Ta 20 Å/NiFe 30 Å/CoFe 20 Å/Cu 28 Å/CoFe 25 Å/MnIr 60 Å/Ta 25 Å) with two ferromagnetic layers, typically a NiFe-based composite, which are separated by a Cu spacer. The Cu spacer is deposited thick enough to prevent any magnetic coupling between the layers. The principle of exchange biasing is then implemented, whereby one of the magnetic layers is coupled to the back layer of antiferromagnetic material. For example, in the structure by Graham et al.

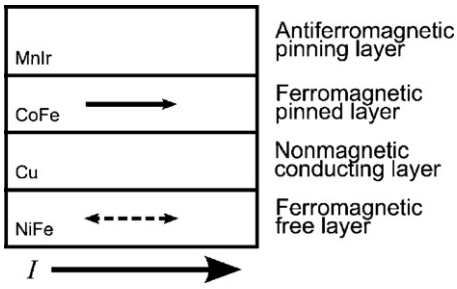

Fig. 6. The basic concept of a spin-valve device. The antiferromagnetic pinning layer forces, or "pins," the magnetization of the adjacent ferromagnetic layer in a particular direction. The nonmagnetic conducting layer is deposited thick enough between the ferromagnetic layers to allow the remaining ferromagnetic layer to freely rotate and detect the presence of external magnetic fields. This form of exchange biasing produces a very sensitive device that exceeds that of AMR and other GMR devices.

(Fig. 6) the MnIr layer forces the magnetization of the CoFe layer in a particular direction. This configuration prevents the rotation of ("pins") the CoFe layer magnetization while allowing the NiFe layer to freely rotate in the presence of external magnetic fields. This form of exchange biasing produces a very sensitive device with a MR ratio range of 6–15% that exceeds that of anisotropic magnetoresistance and other GMR devices (Slaughter et al., 2000). In addition, the sensor by Graham et al. also contains a novel feature—tapered current lines in close proximity to the sensor line to generate on-chip magnetic field gradients. When activated, the current lines are designed to magnetically attract the functionalized magnetic nanoparticles used (250 nm diameter), with the aim of overcoming the slow sedimentation rate for particles of this size in solution and simultaneously concentrating them onto the small-area GMR sensors for detection.

3.1.3.3. Anisotropic magnetoresistance. Before giant magnetoresistance, there was an active pursuit of devices utilizing anisotropic magnetoresistance (McGuire and Potter, 1975). An example of an early AMR stack was Ni–Fe–Co/Ta–N/Ni–Fe–Co. Although AMR devices typically exhibit a MR ratio of around 2% (Slaughter et al., 2000), Miller et al. (2002) "re-introduced" the use of AMR technology in the form of a ring sensor as a way to address the decreasing sensitivity of micron-scale single GMR devices with lateral dimensions caused by fringe-field coupling. In the ring approach (Fig. 7), a single-layer, current-in-plane $Ni_{80}Fe_{20}$ (NiFe) ring sense element is fabricated whereby the AMR material is modulated by the radial fringing field from a single magnetic microbead. The ring sensor has a 5 μm O.D. and 3.2 μm I.D. Like the GMR-based sensor by Baselt et al., the NiFe ring resistance is measured in an AC Wheatstone bridge. When the bead is centered over the ring, the radial fringing field (B) rotates the magnetization from circumferential towards a radial outward direction. This rotation causes a magnetoresistance decrease and a measurable voltage signal in the Wheatstone bridge.

3.1.3.4. Magnetic tunnel junction. Magnetic tunnel junctions (MTJ), also known as tunneling magnetoresistance (TMR) devices, were first demonstrated independently by Moodera et al. (1995) and Miyazaki and Tezuka (1995). Several groups have demonstrated MTJ sensors for micro- to nano-sized magnetic beads (Brzeska et al., 2004; Shen et al., 2005; Wang et al., 2005). MTJs are the most sensitive of the magnetoresistance sensors listed here with a MR ratio of 20–50% (Slaughter et al., 2000), or, as more recently reported, over 200% when using a MgO tunnel barrier (Parkin et al., 2004). Instead of a Cu spacer like that found in the spin-valve construction, MTJs have a thin insulating layer ≤2 nm thick (for aluminum oxide), that acts as a tunnel barrier. The thickness of the insulating layer can

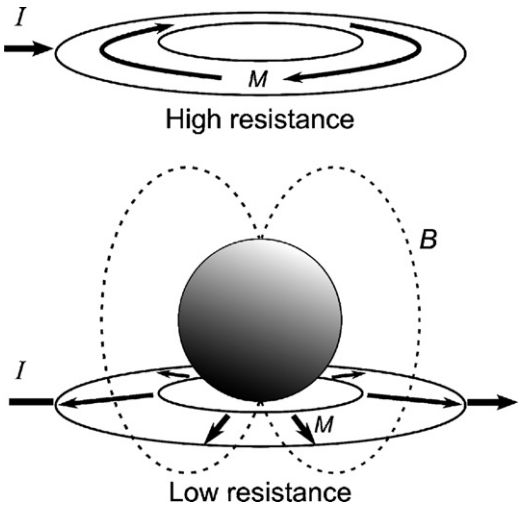

Fig. 7. The basic concept of the AMR ring sensor. A magnetoresistance decrease is achieved when a magnetic bead is centered over the ring such that the radial fringing field (B) rotates the magnetization of the ring from circumferential to a radial outward direction. Electrons pass easier through what is essentially a perpendicular magnetization of the ferromagnetic layer compared to the higher scattering inflicted by circumferential magnetization.

be varied to effectively "tune" the device sensitivity. As an example, Wang et al. used the following stack as proof of concept (Fig. 8): Si/Ta 500 Å/Cu 500 Å/Ta 50 Å/CoFe 18 Å/Ru 7 Å/CoFe 24 Å/Al-O/CoFe 20 Å/Ta 50 Å. Additionally, the sense current is directed perpendicular to the relatively large area MTJ layers rather than in the plane of the sensor as used in GMR structures. Wang et al. are pursuing this concept to produce a 10^6 sensor array called the MagArray™, with the promise of each sensor detecting a single magnetic label (which they call NanoTags) attached to a single DNA fragment.

For further insight into the operation and use of magnetoresistive biosensors, see the earlier reviews by Graham et al. (2004) and Megens and Prins (2005).

3.1.4. Hall effect

3.1.4.1. Silicon Hall sensor. In the classical Hall effect, charge carriers in a current-carrying conductor are pushed to one side of the conductor by the transverse force of an externally applied magnetic field. The charge buildup at the sides of the conductor generates a measurable electric field (or Hall voltage) with a direction perpendicular to both the applied magnetic field and the current. The magnitude of the Hall voltage is given by the equation (Marinace,

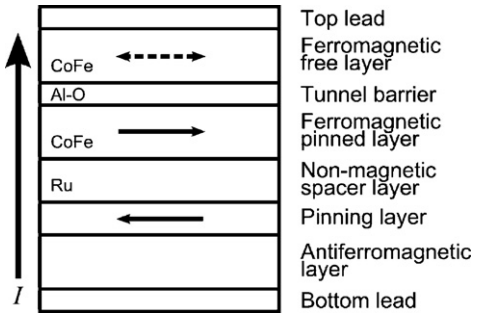

Fig. 8. The basic concept of the MTJ device. Like a spin-valve device, an antiferromagnetic pinning layer is used. However, the spacer layer is a thin insulator that acts as a tunnel barrier whose thickness determines device sensitivity. Additionally, the sense current flows perpendicularly through the MTJ layers rather than in the plane of the device.

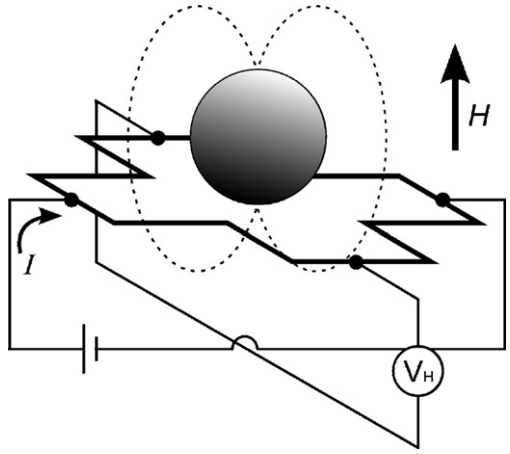

Fig. 9. The basic concept of the Hall cross sensor. Charge carriers in a current-carrying conductor are pushed to one side of the conductor by the transverse force of an externally applied magnetic field, such as that from a magnetic microbead. The charge buildup at the sides of the conductor generates a measurable Hall voltage (V_H) with a direction perpendicular to both the applied magnetic field and the current.

1965),

$$V_H = \frac{IH}{t} R_H, \tag{7}$$

where V_H is the induced Hall voltage that is measured along one of the two axes, I is the current which flows through the other of the two axes in the plane of the Hall region, H is the magnetic field strength along the third axis normal to the Hall region, t is the thickness of the Hall effect region, and R_H is the Hall coefficient. From this equation, it can be seen that the key to the cross-shaped geometry lies in the thickness parameter, t. The thickness of the Hall effect region directly affects the induced Hall voltage: the smaller the region at the intersection of the cross, the larger the Hall voltage. The Hall effect has been utilized by Besse et al. (2002) in a Hall cross sensor fabricated in standard CMOS technology that measures the Hall voltage containing a component proportional to the magnetic induction produced by a magnetic particle, as illustrated in Fig. 9. Additional lock-in electronic circuitry and specific requirements were imposed on the magnetic field applied to the paramagnetic microbead to improve the measured signal-to-noise ratio. Each sensor is approximately the same size as the superparamagnetic bead and therefore capable of detecting a single bead. Recently, a 1024-element array of micron-scale classical Hall sensors has been fabricated and an immunological assay performed with magnetic microbeads (Aytur et al., 2006).

3.2. Indirect detection of magnetic microbeads

In addition to the direct detection of magnetic labels, there have also been attempts to leverage the effects that magnetic particles have on the surroundings as an indirect means to extract pertinent information about a sample. What follows are representative examples of these kinds of technologies that are completely unrelated in their underlying measuring principles, save for the shared requirement for magnetic particles as a critical tool in the biomolecule detection approach.

3.2.1. Micro-cantilever-based Force Amplified Biological Sensor (FABS)

FABS uses a sandwich assay in which antibodies to a known antigen are covalently bound to a *piezoresistive* micro-cantilever

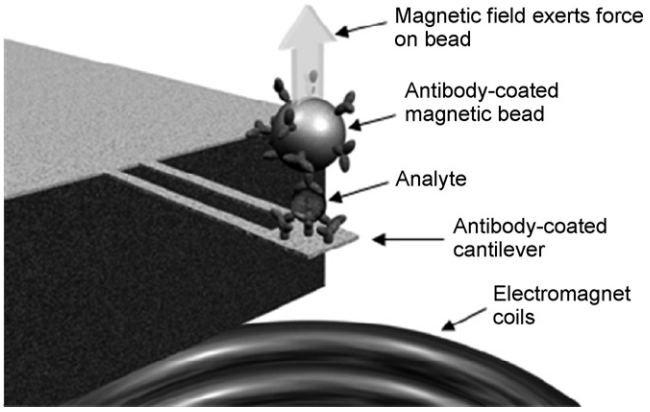

Fig. 10. A 3D cartoon of the FABS device. The assay involves the tethering of magnetic beads, via ligand–receptor interactions, to a micromachined cantilever. When a magnetic field gradient is applied, there is an upward "tug" on the magnetic bead causing a measurable deflection (in pN) of the cantilever.

(Fig. 10), similar in scale to cantilever probes used in an atomic force microscope (AFM) (Baselt et al., 1996). However, instead of monitoring deflected laser light off the cantilever surface as in a standard AFM, FABS utilizes special cantilevers that exhibit a change in resistance due to mechanical stress. When a sample containing the target is flowed over the cantilevers, target molecules are captured on the cantilever by molecular recognition. Captured targets are subsequently labeled by paramagnetic beads. By applying an external magnetic field gradient, the tethered magnetic particles experience a force which causes the cantilever to bend. The bending stress changes the resistance of the piezo micro-cantilever that is measurable using instrumentation based on a Wheatstone bridge circuit. Reports of .07 aM detection limits have been reported using processes that polymerize DNA targets resulting in multiple biotin labels for tethering to avidin-functionalized cantilevers (Weizmann et al., 2004).

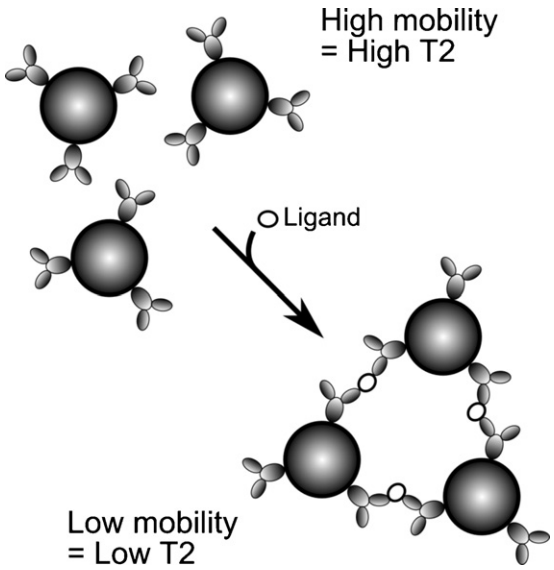

Fig. 11. Nanoparticles, approximately 45 nm in diameter, are used to label and observe ligand–receptor interactions. The superparamagnetic iron-oxide core of each nanoparticle dephases the spins of surrounding water protons and act as magnetic relaxation switches. As the nanoparticles localize into larger groups, they cooperatively enhance the spin–spin relaxation times (lowering the T2) thus providing quantitative data on parameters such as concentration and selectivity.

3.2.2. Magnetic Relaxation Switches (MRS)

This highly sensitive technique is based on nuclear magnetic resonance (NMR) technology that monitors spin–spin relaxation times (T2) of water molecules (Perez et al., 2002). Nanoparticles, approximately 45 nm in diameter, are used to label and observe DNA–DNA, protein–protein, protein–small molecule, or enzyme reactions. As shown in Fig. 11, the superparamagnetic iron-oxide core of each nanoparticle dephases the spins of surrounding water protons and act as magnetic relaxation switches. As the nanoparticles localize into larger groups, they cooperatively enhance the spin–spin relaxation times thus providing quantitative data on parameters such as concentration and selectivity. The particles are polymer encapsulated and the outer surfaces modified to allow the attachment of affinity ligands selected in such a manner as to encourage self-assembly into clusters when ligand–receptor interactions occur. One of the main advantages of this method is that the monitoring of the T2 relaxation time is not dependent on the matrix, or on the presence of nonspecifically bound reagents. Therefore, raw samples, including turbid samples and whole-cell lysates without protein purification, can be analyzed without further processing. Detection in the attomole range has been reported (Grimm et al., 2004).

3.3. Comparing different approaches

The ability to detect a magnetic label in an affinity biosensor is not by itself a useful measure of the effectiveness of an approach. The progression from sample-to-detection will necessarily depend on how the magnetics is integrated with the biochemical assay, including the nature of the sample and its matrix, the sample volume examined, the binding affinities of the capture and label biomolecular recognition moieties (e.g. antibodies), the total binding time, and the fluidics. To date, there are very few such approaches sufficiently advanced to have published assay data suitable for direct comparison. Moreover, there is no single metric for comparing biosensors, because different approaches offer different advantages and limitations for different applications, depending on their implementation, as summarized in Table 1

. For example, some sensing approaches based on very simple sensing devices, such as the frequency-dependent magnetometer, have the potential to achieve analytical sensitivities comparable to colorimetric assays (e.g., ELISA) but faster (minutes versus hours) and at a very low cost per test (Kiely et al., 2007). Another approach is to combine a single magnetic sensor with magnetic forces to rapidly pull labels onto the sensors and thereby reduce typical assay times down to a few minutes for applications where speed is most valued (Janssen et al., 2008). Alternatively, the NRL *cBASS*® combines microfluidics and arrays of relatively large GMR sensors to maximize the analytical sensitivity of multiplexed assays while maintaining short assay times (10's of minutes) and assay simplicity. Finally, solution phase methods such as SQUID-based detection offer their own set of advantages, such as the ability to use nanoparticles to label targets inside living cells.

For solid-phase assays, such as those performed on a sensor chip, one scalable measure of sensitivity that can be compared is the "area per detectable particle" (Rife et al., 2003), as listed in Table 2. When molecular diffusion is the limiting factor in a solid-phase assay, it is well established that the overall sensitivity improves with increasing sensor area (Sheehan and Whitman, 2005). Although much emphasis is often placed on the ability of a sensor to detect the fewest number of labels, often achieved by making the sensors smaller, such emphasis mistakenly neglects the difficulty for target molecules and molecular-scale labels to diffuse and bind to the sensor. Therefore, it is important to distinguish the *density of labels* within the detection area from the *number of labels*, because *the diffusion-limited sensitivity of an assay will be proportional to size of the detection area*. Considering this criterion, approaches that have relatively large detection areas (or volumes) while maintaining the ability to detect relatively few labels should be the most sensitive overall for affinity-based assays. (Note, however, that this criterion is much less important if fluidic, magnetic, or other forces are used to direct target and/or labels to the sensor surfaces.)

4. System integration challenges

It is clearly evident that the detection of magnetic particles can be accomplished by a surprising variety of ingenious methods, but that the overall utility of a system will depend on how the magnetics is integrated with an assay. The remainder of this overview focuses on the approach taken to integrate one such method into an assay system, the NRL *cBASS*®, designed to achieve the maximum analytical sensitivity in a simple, relatively rapid, multiplexed format. This system is based on the detection of magnetic microbead labels by a Bead ARray Counter (BARC®) chip (discussed above), which uses one of the simplest types of solid-state magnetic field sensors to be incorporated into a microelectronic substrate, a GMR wire (Baselt et al., 1998). The *cBASS*® integrates the detection chip with a suite of technologies for microfluidic-based affinity binding assays capable of multiplexed femtomolar (or better) detection of both DNA and proteins in complex matrices in minutes. Specifically, the current system integrates compact magnetics instrumentation, automated microfluidics, reproducible surface chemistry, and a simple assay protocol that can be readily adapted to a wide range of multiplexed assay schemes and microbead detection methods.

4.1. Anatomy of the cBASS® instrumentation

The *cBASS*® instrumentation consists of three main components: the solid-state BARC® sensor chip, a detection electronics module, and a microfluidics module. The underlying principles along with the engineering challenges that guided the integration approach follow.

4.1.1. GMR sensor construction

The third generation BARC®-III sensor chip, originally fabricated by NVE Corp. (under contract to NRL), includes 64 individually addressable multilayer GMR sensors in addition to two reference sensors (Fig. 12). The features and performance of the BARC®-III chip have been discussed in detail in Rife et al. Essentially, each sensor is a magnetic field-dependent resistor trace 1.6 μm wide on a 4.0 μm pitch that follows a serpentine path within a 200 μm-diameter circular area. If stretched out into a straight line, the length of each resistor trace would be 8 mm. The sensors are a multilayer stack of GMR material approximately 33 nm thick whose magnetization naturally lies in the plane of the film, so only the planar components of the field induced in a microbead above a sensor will cause an appreciable magnetoresistance change (Fig. 13).

The diameter of each embedded GMR sensor zone for BARC®-III is 200 μm. One reason this diameter was initially chosen was to accommodate the spot-size capability of the arraying system in use at the time (Sheehan et al., 2003). (As discussed above, however, the size of each sensing zone is also critical in determining the diffusion-related limit of detection versus assay time, so future designs will be based on minimizing this limitation.) Recently, we have teamed with Seahawk Biosystems Corp. and SAE Magnetics to evaluate state-of-the-art GMR sensor designs. Using a proprietary GMR stack design in a configuration similar to the original BARC®-III chip, we have observed a 30-fold increase in sensor signal/bead (unpublished data). This improvement is useful because

Table 1
Survey of magnetic label detection technologies

Detector type	Potential advantages	Special operational parameters
Maxwell bridge (see Section 3.1.1)	Simple instrumentation Well suited for handheld system No substrate surface preparation required Real-time measurement Uses ferromagnetic particles which are easier to detect	Liquid phase assay (ferrofluid) Single analyte (immunoassay centric) Magnetic labels are custom coated Long assay incubation time Uses relatively large sample volume Narrow dynamic range Slow response time $21 \pm 4\,\mu V/(\mu g\ Fe/mL)$
Resonant coil (see Section 3.1.1)	Well suited for handheld system Uses disposable plastic strips on which assays are performed and measured Potential for multiplexing target samples Uses commercially available paramagnetic particle labels	Solid-phase assay More complex circuitry (phase-locked loop) compared to Maxwell bridge Frequency measurement requires stable oscillation circuit Sensitivity is dependent on coil geometry and internal dimensions Narrow linear dynamic range
SQUID (see Section 3.1.2)	Single nanoparticle detection under "cold sample" conditions High T_c-SQUID ("warm sample") allows sample to remain at room temperature Removal of unbound magnetic labels from sample is not necessary	Solid or liquid phase assays Single nanoparticle detection requires samples be cooled to ~77 K High T_c-SQUID has lower sensitivities (cf. 5×10^4, 56 nm particles) High T_c-SQUID sensitivity is dependent on distance (μm) of super cooled detector from room temperature sample Sophisticated measurement instrumentation Requires shielding from electromagnetic interference Relatively large device footprint Demanding power requirements
GMR (see Section 3.1.3)	Large particle label-to-sensor ratio Integrated circuit fabrication technology Flexible sensor geometries Can be deployed in various measurement system formats (e.g. benchtop, portable field use) Analyte multiplexing Probe arraying methods are similar to standard microarray technology Various means available to reduce nonspecifically bound magnetic labels	Solid or liquid phase assays Better S/N with small sensor passivation layer thickness relative to label diameter Uses sensitive detection electronics for improved S/N Uses specialized semiconductor fabrication steps Requires effective surface biofunctionalization to reduce non-specific binding Detection of one magnetic label depending on particle size and sensor geometry
Hall sensor (see Section 3.1.4)	Capable of single particle detection (if sensor is on size scale of particle) Integrated circuit fabrication technology Can be fabricated as arrays Analyte multiplexing	Solid or liquid phase assays Increased Hall sensor voltage inversely related to thickness of Hall effect region Sensor size on scale of magnetic particle; will need to consider an array for quantitative measurements Diffusion limits must be considered because of small sensor size Long incubation periods Substantial dead space between sensors in array format Multiplexing electronics to address 1000 of sensors Special consideration for removal of nonspecifically bound particles
Microcantilever (see Section 3.2)	Cantilevers produced by established microlithographic techniques (MEMS) Measurement electronics well established (e.g. optical, piezoelectric feedback) Suited for benchtop or portable system	Solid or liquid phase assays Analyte multiplexing (genomic or immuno assays) Indirect measurement via mechanical movement of cantilever to external magnetic pull on magnetic labels Uses sensitive detection electronics for improved S/N Requires effective surface biofunctionalization to reduce non-specific binding Assay must be controlled to occur only on one side of the cantilever Sensitive to environmental conditions (temperature, vibration, etc.)

Table 1 (*Continued*)

Detector type	Potential advantages	Special operational parameters
MRS (see Section 3.2)	Samples can be tested in an array format using standard 384-well plates	Liquid phase assay
	Small samples volumes (μL)	Genomic and immuno assays
	Environmentally robust (sample is independent of temperature, turbidity)	Highly dependent on particle cluster formation
	Entirely liquid phase; no surface preparation required, minimal sample prep	Requires NMR techniques and instrumentation (i.e. T1, T2 spin echo sequences, superconducting magnet)
	No PCR required	Primarily confined to the laboratory
	Faster biomolecular kinetics since there is no substrate immobilization involved	
	Capable of detecting single-nucleotide mismatches	

Table 2
Magnetic label detection capabilities

Detector type	Detection area (μm^2)	Particle	Particle diameter (μm)	Sensitivity (particles)	Area per detectable particle (μm^2)	Ref.
Maxwell bridge[a]	–	Ferrofluid	.11 (mean)	–	–	Kriz et al. (1996)
Resonant coil	2.5×10^7	Dynal M-280	2.8	10^5	2.5×10^2	Richardson et al. (2001)
SQUID	2.0×10^7	Magnetite	.025	7×10^5	27.8	Enpuku et al. (2005)
GMR (BARC®-III)	3.1×10^4	Dynal M-280	2.8	10	3.1×10^3	Baselt et al. (1998)
GMR	3.8×10^3	Bangs	.35 (mean)	2.0×10^3	1.9	Schotter et al. (2004)
Spin-valve	12	Micromer®-M	2.0	1	12	Graham et al. (2002)
AMR ring	8.0	$Ni_{30}Fe_{70}$	4.3	1	8.0	Miller et al. (2002)
MTJ/TMR	10	Magnetite	.016	1	10	Wang et al. (2005)
Hall sensor	5.8	Dynal M-280	2.8	1	5.8	Besse et al. (2002)
Microcantilever	2×10^4	NdFeBLa	2.0 (mean)	1	2×10^4	Baselt et al. (1996)
MRS[a]	–	Magnetite	.045	–	–	Perez et al. (2002)

[a] Volumetric measurement.

it lowers the field required to induce a detectable moment in the bead labels, thereby lowering the power requirement for the associated electromagnet, and reducing the gain required to read each sensor; the implications of this improvement are discussed below.

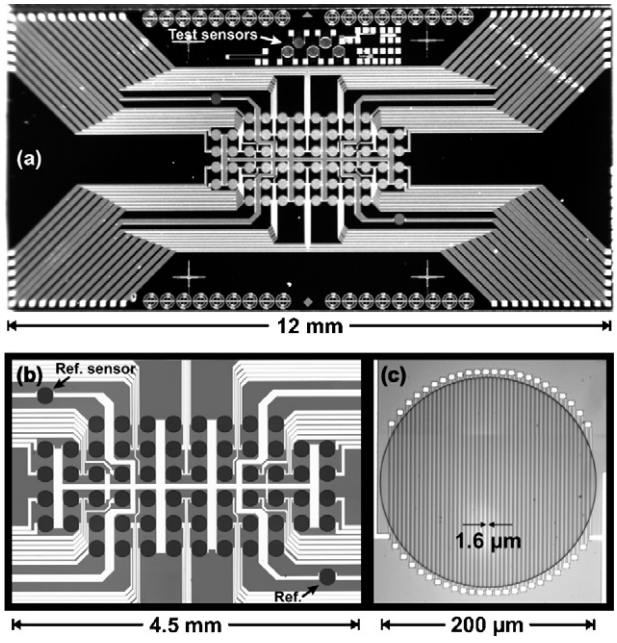

Fig. 12. Micrograph of BARC®-III chip (Rife et al., 2003). (a) The 68 pin-out chip, including a central sensing area with 64 sensors and two reference sensors, and a number of test structures. (b) Closer view of the central sensing area. (c) Close-up of one serpentine GMR sensor trace encompassing a 200 μm-diameter sensing zone.

4.1.2. Instrumentation design and bead detection with GMR sensors

Design of the detection electronics relies heavily on low-level measurement electronics for routine detection of the microvolt or nanovolt signal generated by a GMR sensor chip while it is subjected to various sources of noise (Johnson, $1/F$ or flicker, etc.). Despite the need for sophisticated electronics to obtain the working signal, the basic design is based on the Wheatstone bridge. To obtain an optimal electronic signal-to-noise ratio, a "reference" GMR sensor that is identical to the main "signal" sensor is used. The two sensors comprise half of a Wheatstone bridge. To enable lock-in detection of the magnetic beads on top of each GMR sensor, a 200 Hz, 80–400 Oe RMS modulated magnetic field is applied along the z-axis (nor-

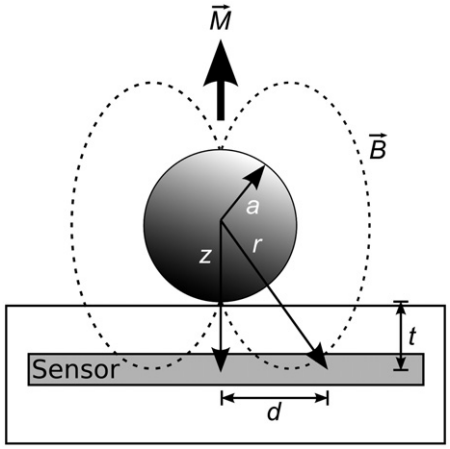

Fig. 13. Schematic of magnetic fields induced in a paramagnetic bead over a GMR sensor.

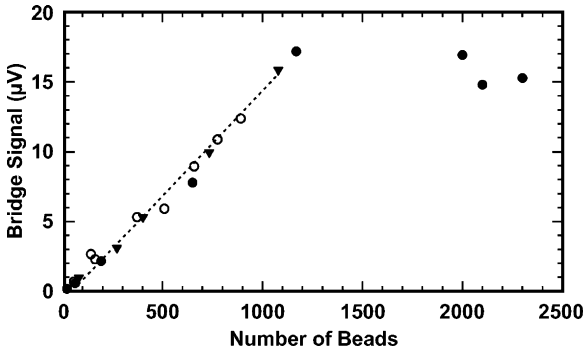

Fig. 14. The BARC®-III sensor signal versus bead number.

mal to the sensor; Fig. 13), using a custom designed electromagnet integrated with the chip and fluidics cartridge.

Each sensor (signal and reference) on the chip is basically a wire whose resistance changes ($\Delta R/R$) in response to the strength of an externally induced in-plane magnetic field (B_X). The electronic detection of magnetic microbeads on the GMR sensors (Baselt et al., 1998; Miller et al., 2001) can be summarized as follows (see Fig. 13): an external AC magnetic field, H_Z^0, is applied normal to the chip (the z-direction). An individual bead, magnetized by the external field and resting on the surface above the GMR resistor trace, generates an ac local dipole field, B, with in-plane components sufficient to cause a magnetoresistance change. The single bead magnetic field components, B_X, directed positively and negatively along the GMR trace both contribute to a reduction in overall sensor resistance. The resistance changes of the individual beads are independent and additive up to a saturation point (Fig. 14), where the dipole fields of adjacent beads act to reduce the effective applied field (Rife et al., 2003). The AC change in resistance, $\Delta R/R$, generates an ac voltage change across a DC-biased Wheatstone bridge. The bridge voltage signal is filtered to remove the DC component, amplified $\sim 10^2$ to 10^4 times, and detected by a lock-in amplifier synchronized with the applied AC magnetic field. Note that the external field should not be applied until after the beads have settled on the chip and the assay has been completed, otherwise undesirable interactions (e.g. clustering) will occur between the magnetized beads. In addition, the DC bias on the bridge cannot be too high ($\leq$10 V in our case) or electrical breakdown can occur between the electrolyte and the submicron surface passivation layer, destroying the device.

4.1.3. Magnitude and noise of bead detection

The magnetic field from each microbead is highly localized over the GMR sensor. Despite the large difference in size between a bead and a sensor wire, single microbeads can be readily detected (Baselt et al., 1998; Edelstein et al., 2000). The overall GMR signal for a sensor, $\Delta R/R$, is determined by sensor geometry and the cumulative local magnetoresistance changes associated with individual microbeads, and has been analyzed in detail for the BARC® GMR sensors (Miller et al., 2001; Rife et al., 2003). The analysis shows that the signal-to-noise generally improves with increases in the following factors: (1) DC voltage bias on the Wheatstone bridge; (2) sharpness of the GMR magnetoresistance response around zero field; (3) bead-to-sensor area ratio; (4) bead magnetization; and with a decrease in bead-sensor distance (achieved by decreasing the thickness of the chip surface passivation layer). Note that other solid-state magnetic detection techniques should follow similar relationships. For example, GMR sensors such as spin-valves with a magnetoresistance response that proportional to B (instead of B^2) would have a correspondingly weaker dependence on bead magnetization and passivation layer thickness.

The electronic sources of noise are $1/F$ noise and Johnson noise. For the original BARC®-III GMR sensors, $1/F$ noise dominates at low frequencies and falls off to a knee at the Johnson noise floor beyond 1.5 kHz. $1/F$ noise is greater for smaller volume sensors, scaling as $1/(FwL)^{1/2}$. The $1/F$ electronic signal-to-noise (S/N) then becomes independent of the area of the GMR sensor (Rife et al., 2003). Correspondingly, the Johnson noise scales as $(L/w)^{1/2}$, so that the Johnson electronic S/N is proportional to $1/(w^{1/2}L^{3/2})$. As discussed in above, however, in an assay the overall analytical detection S/N is a convolution of the binding assay sensitivity (which determines the number of beads/sensor) with the sensor S/N, such that larger sensors are favored. This convolution is important up to the point where the electronic noise because less than the variance from assay-to-assay associated with nonspecifically bound labels (the assay "noise"). We find a 200 μm diameter sensor zone is approximately that size; i.e., the overall detection S/N is typically limited by the assay variance, not the GMR sensor performance.

4.1.4. Fluidics system

The fluidic system has the critical role of automating the reproducible, controlled flow of microliters of sample and reagent fluids across the sensor chip surface. Moreover, the fluids must be evenly dispersed across the sensor chip so that all elements in the sensor array are uniformly exposed. In addition, the use of magnetic labeling and detection requires that all materials be fabricated from nonmagnetic components and that large metallic components be avoided (to prevent eddy current heating by the AC magnetic fields). Another complication is the integral use of micron-scale particles, which requires that all components be resistant to clogging. Other objectives include ease of fabrication, compatibility of the fluidics wall materials with the assay biochemistry, and minimal carryover contamination between assays. These requirements will generally apply to all other magnetic label detection techniques.

The component with the most stringent requirements for successful assays is the flow cell mounted on the sensor chip. Uniformity is critical for assay-to-assay consistency because if a certain sensor were, for example, to receive significantly more beads than another, it would register a false positive or negative. The problem is compounded by the disparity between the exit diameter of the inlet tube from the microfluidic network and the width of the sensor array (i.e. exit tube diameter « width of sensor array). The uniformity of the analyte dispersion across the GMR sensors was assessed with fluid flow models (Tamanaha et al., 2002). Numerical finite-element analysis (FEA) simulations produced several feasible solutions, the simplest effective channel geometry being one in which a narrow inlet channel gradually expands from the inlet tube to the wider cross-sectional area of the flow cell. Under laminar flow conditions, this geometry creates a velocity profile that is symmetric along the central flow axis with a flattened parabolic leading edge across the width of the flow cell and more parabolic across the smaller height. Such a velocity profile has been a consistent design feature incorporated in all flow cells produced for *cBASS*®. The fluidics cell has evolved to become part of a "press-together" assay cartridge that has been engineered for one-step assembly, or replacement, of the sensor chip without the need for permanent adhesives.

The current *cBASS*® integrates a number of commercial off-the-shelf fluidic components in a single instrument for a completely automated fluidics solution. Major components include a valve switcher (Rheodyne LLC) for sample and reagent selection, a miniature peristaltic pump (Instech Laboratories, Inc.) in negative pressure mode to regulate fluid flow rate through the microfluidic cell, and a miniature portable motor and pump unit (Drummond Scientific Co.) for resuspension of the magnetic microbead solu-

tion when settling has occurred. The fluid connection port between the cartridge is based on a simple compression fitting to allow rapid switching between different cartridges when inserted in the cBASS® reader.

4.2. Assays and fluidic force discrimination

As for many other biomolecular labels, magnetic labeling can be similarly accomplished using specific ligand–receptor interactions. A typical "sandwich" type assay proceeds as follows:

1. Receptor molecules specific for the target biomolecules are attached to the surface of a solid substrate. Often arrays of different probe spots are used to simultaneously detect multiple targets.
2. When target molecules are present in a sample solution, they are captured at the surface.
3. Magnetic particles coated with a second set of receptor molecules for the target are introduced, labeling the previously captured targets.
4. The label particles are detected by a magnetic sensor.

Sandwich assays are commonly performed using antibody–antigen pairs and complementary DNA strands, and often use the strongly binding biomolecular combination of streptavidin and biotin to attach the receptor molecules to the bead or substrate surface.

In practice, one of the biggest problems plaguing not only label-based assays, but assays in general, is nonspecific binding of target and/or labels. Many mitigation strategies have been employed to address this problem, the most popular being the modification of the substrate surface with a nonfouling passivation layer such as polyethylene glycol (PEG), and/or blocking with proteins (e.g. BSA, casein) and surfactants (e.g. Triton-X, Tween 20).

The overall performance of the assay ultimately relies on the ability to discriminate against false-positives. Addressing nonspecific binding is where the use of *micron*-scale particles as labels provides significant advantages when combined with microfluidics. Typical labels used in bioassays are generally molecular or nanoscale in size in order to match the size of the biomolecular recognition probes and analyte targets. Conventional wisdom, therefore, has discounted micrometer-scale labels—such as magnetic microbeads used for magnetic separation and as assay substrates—based on concerns about their large relative size (Graham et al., 2004; Wang et al., 2005). However, microbead labels with polymer or other coating matrices offer a number of distinct advantages over smaller labels. They can encapsulate a high density of detectable label material and therefore are easier to observe by routine optical microscopy (Lee et al., 2000; Mulvaney et al., 2004, 2007) or magnetic detection (Rife and Whitman, 2004; Rife et al., 2003). A microbead surface can also be functionalized for specific molecular recognition with a higher total number of receptors, improving the labeling efficiency, while still able to label a *single* molecular recognition event at a capture surface. Finally, if a controlled laminar flow is maintained at the capture surface, fluidic drag forces applied to a microbead labels can be used to preferentially remove nonspecifically bound labels and thereby dramatically improve the assay performance (Mulvaney et al., 2007; Rife and Whitman, 2004).

4.2.1. Reducing nonspecific binding by force discrimination

To improve the detection of specific versus nonspecific biochemical interactions, one can exploit the difference in interaction forces, or binding affinity, by applying a controlled force to remove weakly bound molecules, or the labels (i.e. beads) they are attached to, while leaving behind specifically-bound ligand–receptor pairs of interest. One way to accomplish this discrimination is by applying an external magnetic force from an inhomogeneous magnetic field gradient to pull away the bead labels magnetically. This technique is known as magnetic force discrimination, an assay method introduced by NRL (Baselt et al., 1996; Lee et al., 2000). However, with current commercially-available paramagnetic microbeads and simple magnetic geometries, magnetic forces are limited to ~1 pN; therefore, the nonfouling properties of the substrate must be very tightly controlled for this approach to be consistently effective.

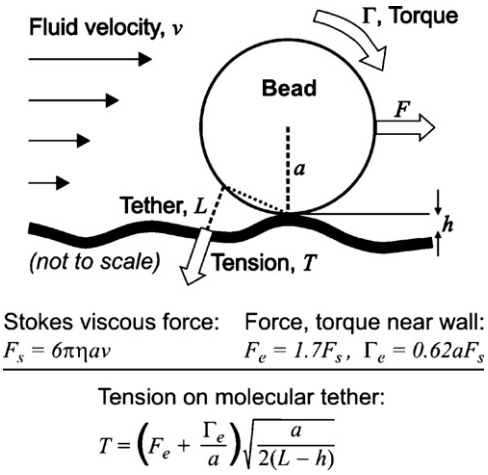

Fig. 15. The biophysics of fluid force discrimination (FFD).

An alternative and more reliable means for removal of nonspecifically-bound microbead labels is the application of fluid force under laminar flow, an approach known as Fluid Force Discrimination™ (FFD) (Mulvaney et al., 2007). When applied in microchannels under laminar flow conditions, fluidic forces up to several hundred pN are possible, thereby offering ability reliable method to improve microbead binding assays. The force applied to a microbead during FFD is a function of the flow velocity, channel geometry, buffer viscosity, and bead diameter, but can be estimated from the viscous Stokes force and torque (Chang and Hammer, 1996; Goldman et al., 1967; Rife and Whitman, 2004). As illustrated in Fig. 15, for a bead tethered to a surface by molecular interactions, the tension force on the tether is much larger than the simple Stokes force, because the offset between the bead-surface contact point and the bead-tether contact point creates a mechanical lever. For example, with a 1.4 μm-radius bead attached by a 10 nm-long tether in a flow cell 250 μm high × 800 μm wide, a flow rate of 33 μL/min produces a tension force ~48 pN. Although the flow rate needed to remove a microbead depends on a number of variables, the wide range of forces accessible with micron-scale beads and reasonable microfluidic flow rates (up to 100 μL/min) makes it straight forward in practice to determine an effective rate and duration for FFD.

Because the laminar flow velocity is zero at the surface, the force decreases rapidly with bead radius (as $a^{5/2}$), such that a 100 nm-radius bead under these conditions would exert a tension force ≪ 0.1 pN. Therefore, FFD is not possible with nanoparticle labels for any practical microfluidic flow rates. Effective fluidic force discrimination also cannot be achieved by simple wash steps (e.g. the jet of water from a typical lab wash bottle), because non-uniform and/or turbulent flows induce a wide range of uncontrolled forces, leading to random and indiscriminant label removal.

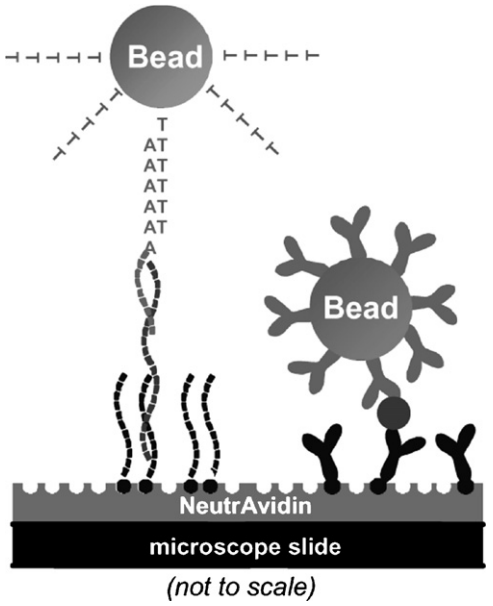

Fig. 16. Solid-phase hybridization assay and immunoassay schemes on biofunctionalized substrate used in the NRL *cBASS*®.

4.2.2. Fluidic force discrimination assays with magnetic microbeads

The basic schemes for "sandwich" type FFD assays as currently implement in *cBASS*® are illustrated in Fig. 16 (Mulvaney et al., 2007; Stine et al., 2007). For all assay schemes, following target capture (and secondary labeling, if required), the capture surface is exposed to a high density of microbeads, thereby labeling those locations where target molecules are bound to the surface. We then briefly introduce a controlled laminar flow of buffer across the surface, applying a drag force on each bead that is less than the rupture strength of a specific DNA duplex (approx. 800–1200 pN) (Lee et al., 1994) or immunochemical complex (approx. 60–250 pN) (Kaur et al., 2004), but greater than that required to remove beads bound to the surface by weak, nonspecific interactions (approx. 0.1–10 pN).

An implementation of FFD for multiplexed ssDNA detection is demonstrated in the optical micrographs shown in Fig. 17. In this assay, three different capture probes were immobilized on the substrate, as follows: a positive control spot for microbead binding (biotinylated oligo$(dA)_{25}$); a capture probe complementary to the target (two spots); and a noncomplementary capture probe (two spots). The left micrographs (0 μL/min) show the surface after hybridization with the target (10 nM) and the introduction of 2.8 μm-diameter microbead labels (Dynal M-280). The right micrographs show the surface following FFD (33 μL/min), where the specific label density is more than 100 times greater than the nonspecific background. Notably, the background on the noncomplementary capture probe spots is indistinguishable to that on the surrounding NeutrAvidin™ substrate (chosen specifically for its nonfouling properties). As the flow rate (and force) is further increased, specifically bound beads are eventually removed, demonstrating the effectiveness of laminar fluidic forces for fully controlling microbead-labeled binding assays.

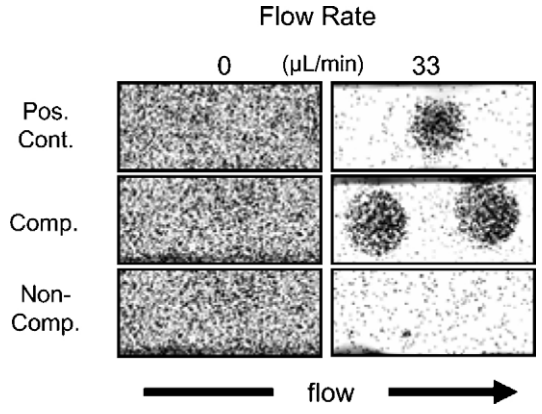

Fig. 17. Implementation of fluidic force discrimination for multiplexed ssDNA detection. See text for a complete description of the assay.

5. Conclusion

Magnetic labeling and detection are emerging as important components in bioassay systems because of their many advantages, especially the absence of a magnetic background in biological samples. Although much of the work in the past has focused on the development of sensing methodology, magnetic label-based assays are now being incorporated into more comprehensive instruments that incorporate sample fluidics. Often such platforms are designed principally around relatively mature magnetic detection systems. However, successful development of commercial biosensing platforms based on magnetic labeling and detection will require the integration of these technologies into systems specifically designed to *optimize the performance of the overall assay from sample-to-answer,* which may require redesigning the magnetics. With continued advances in microfluidics, microtechnologies, and microsystems integration, magnetic labeling and detection-based systems are poised to become important players in the diverse biosensing marketplace.

Acknowledgements

This work was supported by the Office of Naval Research and a Cooperative Research and Development Agreement with Seahawk Biosystems, Inc. (NCRADA-NRL-04-341). Author S.P.M. is an employee of Nova Research Inc., 1900 Elkins St. Suite 230, Alexandria VA 22308 USA.

References

Aytur, T., Foley, J., Anwar, M., Boser, B., Harris, E., Beatty, P., 2006. J. Immunol. Methods 314, 21–29.
Baeumner, A.J., 2003. Anal. Bioanal. Chem. 377, 434–445.
Baibich, M.N., Broto, J.M., Fert, A., Vandau, F.N., Petroff, F., Eitenne, P., Creuzet, G., Friederich, A., Chazelas, J., 1988. Phys. Rev. Lett. 61, 2472–2475.
Baselt, D.R., Lee, G.U., Colton, R.J., 1996. J. Vac. Sci. Technol. B 14, 789–793.
Baselt, D.R., Lee, G.U., Natesan, M., Metzger, S.W., Sheehan, P.E., Colton, R.J., 1998. Biosens. Bioelectron. 13, 731–739.
Besse, P.A., Boero, G., Demierre, M., Pott, V., Popovic, R., 2002. Appl. Phys. Lett. 80, 4199–4201.
Binasch, G., Grunberg, P., Saurenbach, F., Zinn, W., 1989. Phys. Rev. B 39, 4828–4830.
Black, R.C., Wellstood, F.C., Dantsker, E., Miklich, A.H., Nemeth, D.T., Koelle, D., Ludwig, F., Clarke, J., 1995. Appl. Phys. Lett. 66, 99–101.
Brzeska, M., Panhorst, M., Kamp, P.B., Schotter, J., Reiss, G., Puhler, A., Becker, A., Bruckl, H., 2004. J. Biotechnol. 112, 25–33.
Calvin, S., Miller, M.M., Goswami, R., Cheng, S.F., Mulvaney, S.P., Whitman, L.J., Harris, V.G., 2003. J. Appl. Phys. 94, 778–783.
Caruso, M.J., Bratland, T., Smith, C.H., Schneider, R., 1998. Sensors. Retrieved 26 October 2006, from http://archives.sensorsmag.com/articles/1298/mag1298/index.htm.
Chang, K.C., Hammer, D.A., 1996. Langmuir 12, 2271–2282.
Chemla, Y.R., Crossman, H.L., Poon, Y., McDermott, R., Stevens, R., Alper, M.D., Clarke, J., 2000. Proc. Natl. Acad. Sci. USA 97, 14268–14272.
Dieny, B., Speriosu, V.S., Parkin, S.S.P., Gurney, B.A., Wilhoit, D.R., Mauri, D., 1991. Phys. Rev. B 43, 1297–1300.
Dreyer, W.J., 1974. Immunological reagent and radioimmuno assay. United States Patent No. 3853987. Washington, DC: U.S. Patent and Trademark Office.
Edelstein, R.L., Tamanaha, C.R., Sheehan, P.E., Miller, M.M., Baselt, D.R., Whitman, L.J., Colton, R.J., 2000. Biosens. Bioelectron. 14, 805–813.

Enpuku, K., Inoue, K., Soejima, K., Yoshinaga, K., Kuma, H., Hamasaki, N., 2005. IEEE Trans. Appl. Superconduct. 15, 660–663.
Farre, M., Barcelo, D., 2003. TRAC 22, 299–310.
Gao, X., Mathieu, H.J., Schawaller, M., 2004. Surf. Interface Anal. 36, 1507–1512.
Goldman, A.J., Cox, R.G., Brenner, H., 1967. Chem. Eng. Sci. 22, 653–660.
Graham, D.L., Ferreira, H., Bernardo, J., Freitas, P.P., Cabral, J.M.S., 2002. J. Appl. Phys. 91, 7786–7788.
Graham, D.L., Ferreira, H.A., Feliciano, N., Freitas, P.P., Clarke, L.A., Amaral, M.D., 2005. Sens. Actuators B 107, 936–944.
Graham, D.L., Ferreira, H.A., Freitas, P.P., 2004. Trends Biotechnol. 22, 455–462.
Grimm, J., Perez, J.M., Josephson, L., Weissleder, R., 2004. Cancer Res. 64, 639–643.
Hindson, B.J., Makarewicz, A.J., Setlur, U.S., Henderer, B.D., McBride, M.T., Dzenitis, J.M., 2005. Biosens. Bioelectron. 20, 1925–1931.
Hunt, R.P., 1971. IEEE Trans. Magnetics MAG7, 150–154.
Janssen, X.J.A., van IJzendoorn, L.J., Prins, M.W.J., 2008. Biosens. Bioelectron. 23, 833–838.
Kaur, J., Singh, K.V., Schmid, A.H., Varshney, G.C., Suri, C.R., Raje, M., 2004. Biosens. Bioelectron. 20, 284–293.
Kiely, J., Hawkins, P., Wraith, P., Luxton, R., 2007. IET Sci. Meas. Technol. 1, 270–275.
Kotitz, R., Matz, H., Trahms, L., Koch, H., Weitschies, W., Rheinlander, T., Semmler, W., Bunte, T., 1997. IEEE Trans. Appl. Superconduct. 7, 3678–3681.
Kriz, C.B., Radevik, K., Kriz, D., 1996. Anal. Chem. 68, 1966–1970.
Lee, G.U., Chrisey, L.A., Colton, R.J., 1994. Science 266, 771–773.
Lee, T.S., Dantsker, E., Clarke, J., 1996. Rev. Sci. Instrum. 67, 4208–4215.
Lee, G.U., Metzger, S., Natesan, M., Yanavich, C., Dufrene, Y.F., 2000. Anal. Biochem. 287, 261–271.
Li, G.X., Joshi, V., White, R.L., Wang, S.X., Kemp, J.T., Webb, C., Davis, R.W., Sun, S.H., 2003. J. Appl. Phys. 93, 7557–7559.
Li, G.X., Sun, S.H., Wilson, R.J., White, R.L., Pourmand, N., Wang, S.X., 2006. Sens. Actuators A 126, 98–106.
Marinace, J.C., 1965. High sensitivity hall effect probe. United States Patent No. 3202913. Washington, DC: U.S. Patent and Trademark Office.
McGuire, T.R., Potter, R.I., 1975. IEEE Trans. Magn. 11, 1018–1038.
Megens, M., Prins, M., 2005. J. Magn. Magn. Mater. 293, 702–708.
Miller, M.M., Prinz, G.A., Cheng, S.F., Bounnak, S., 2002. Appl. Phys. Lett. 81, 2211–2213.
Miller, M.M., Sheehan, P.E., Edelstein, R.L., Tamanaha, C.R., Zhong, L., Bounnak, S., Whitman, L.J., Colton, R.J., 2001. J. Magn. Magn. Mater. 225, 138–144.
Miyazaki, T., Tezuka, N., 1995. J. Magn. Magn. Mater. 139, L231–L234.
Moodera, J.S., Kinder, L.R., Wong, T.M., Meservey, R., 1995. Phys. Rev. Lett. 74, 3273–3276.
Mulvaney, S.P., Cole, C.L., Kniller, M.D., Malito, M., Tamanaha, C.R., Rife, J.C., Stanton, M.W., Whitman, L.J., 2007. Biosens. Bioelectron. 23, 191–200.
Mulvaney, S.P., Mattoussi, H.M., Whitman, L.J., 2004. Biotechniques 36, 602–609.
Néel, L., 1949. Ann. Geophys. 5, 99–136.
Parkin, S.S.P., Kaiser, C., Panchula, A., Rice, P.M., Hughes, B., Samant, M., Yang, S.H., 2004. Nat. Mater. 3, 862–867.
Pearson, J.E., Gill, A., Vadgama, P., 2000. Ann. Clin. Biochem. 37, 119–145.
Perez, J.M., Josephson, L., O'Loughlin, T., Hogemann, D., Weissleder, R., 2002. Nat. Biotechnol. 20, 816–820.
Prestvik, W.S., Berge, A., Mork, P.C., Stenstad, P.M., Ugelstad, J., 1997. In: Häfeli, U., Schütt, W., Teller, J., Zborowski, M. (Eds.), Scientific and Clinical Applications of Magnetic Carriers. Plenum Press, New York, pp. 11–35.
Richardson, J., Hill, A., Luxton, R., Hawkins, P., 2001. Biosens. Bioelectron. 16, 1127–1132.
Rife, J.C., Miller, M.M., Sheehan, P.E., Tamanaha, C.R., Tondra, M., Whitman, L.J., 2003. Sens. Actuators A 107, 209–218.
Rife, J.C., Whitman, L.J., 2004. Fluidic force discrimination. Patent Application No. 20040253744. Washington, DC: U.S. Patent and Trademark Office.
Schotter, J., Kamp, P.B., Becker, A., Puhler, A., Brinkmann, D., Schepper, W., Bruckl, H., Reiss, G., 2002. IEEE Trans. Magn. 38, 3365–3367.
Schotter, J., Kamp, P.B., Becker, A., Puhler, A., Reiss, G., Bruckl, H., 2004. Biosens. Bioelectron. 19, 1149–1156.
Sheehan, P.E., Edelstein, R.L., Tamanaha, C.R., Whitman, L.J., 2003. Biosens. Bioelectron. 18, 1455–1459.
Sheehan, P.E., Whitman, L.J., 2005. Nano Lett. 5, 803–807.
Shen, W.F., Liu, X.Y., Mazumdar, D., Xiao, G., 2005. Appl. Phys. Lett. 86, 253901-1–253901-3.
Slaughter, J.M., Chen, E.Y., Whig, R., Engel, B.N., Janesky, J., Tehrani, S., 2000. JOM-e 52. Retrieved 23 October 2006, from http://www.tms.org/pubs/journals/JOM/0006/Slaughter/Slaughter-0006.html.
Stine, R., Cole, C.L., Ainslie, K.M., Mulvaney, S.P., Whitman, L.J., 2007. Langmuir 23, 4400–4404.
Tamanaha, C.R., Whitman, L.J., Colton, R.J., 2002. J. Micromech. Microeng. 12, N7–N17.
Thomson, W., 1857. Proc. R. Soc. Lond. 8, 546–550.
Tsukamoto, A., Saitoh, K., Suzuki, D., Sugita, N., Seki, Y., Kandori, A., Tsukada, K., Sugiura, Y., Hamaoka, S., Kuma, H., Hamasaki, N., Enpuku, K., 2005. IEEE Trans. Appl. Superconduct. 15, 656–659.
Vo-Dinh, T., Cullum, B., 2000. Fresenius J. Anal. Chem. 366, 540–551.
Wang, S.X., Bae, S.Y., Li, G.X., Sun, S.H., White, R.L., Kemp, J.T., Webb, C.D., 2005. J. Magn. Magn. Mater. 293, 731–736.
Weizmann, Y., Patolsky, F., Lioubashevski, O., Willner, I., 2004. JACS 126, 1073–1080.